

An Efficient and Accurate Method to Solve Low Frequency and Non-Conformal Problems Using Finite Difference Time Domain (FDTD)

Kadappan Panayappan¹ and Raj Mittra^{1, 2, *}

(Invited Paper)

Abstract—In this article we present ν FDTD (New FDTD), an efficient and accurate method for solving low frequency problems and with those non-conformal geometries by using the Finite Difference Time Domain (FDTD) method. The conventional time domain technique FDTD demands extensive computational resources when solving low frequency problems, or when dealing with dispersive media. The ν FDTD technique is a new general-purpose field solver, which is designed to tackle the above mentioned issues using some novel approaches, which deviate significantly from the legacy methods that only rely on minor modifications of the FDTD update algorithm. The ν FDTD solver is a hybridized version of the conformal FDTD (CFDTD), and a novel frequency domain technique called the Dipole Moment (DM) approach. This blend of time domain and frequency domain techniques empowers the solver with potential to solve problems that involve: (i) calculating low frequency response accurately and numerically efficiently; (ii) handling non-Cartesian geometries such as curved surfaces accurately without staircasing; (iii) handling thin structures, with or without finite losses; and (iv) dealing with multi-scale geometries.

1. INTRODUCTION

The conventional time domain technique FDTD demands extensive computational resources when solving low-frequency problems, or when dealing with dispersive media. To tackle some of these challenges, the conventional techniques are often modified in a manner that is tailored to solve a particular problem of interest. However, more often than not, these tailored methods turn out to be computationally expensive, and they often lead to instabilities. Hence, it is useful to develop techniques that can overcome the above limitations, while preserving the advantages of the existing methods. The ν FDTD (New FDTD) technique, which is described in this chapter, is a new general-purpose field solver, which is designed to tackle the above issues by using some novel approaches, which deviate significantly from the legacy methods that only rely on minor modifications of the FDTD update algorithm to address the problems.

2. ν FDTD SOLVER

The ν FDTD solver [1] is a hybridized version of conformal FDTD (CFDTD) [2], and a novel frequency domain technique called the Dipole Moment (DM) approach described in [1, 3]. This blend of time domain and frequency domain techniques empowers the solver with potential to solve problems that require:

Received 14 January 2015, Accepted 26 February 2015, Scheduled 1 March 2015

* Corresponding author: Raj Mittra (rajmittra@ieee.org).

¹ Electromagnetic Communication Lab, Pennsylvania State University, USA. ² University of Central Florida, USA.

- Calculating low frequency response accurately and numerically efficiently
- Handling non-Cartesian geometries such as curved surfaces accurately without staircasing
- Handling thin structures, with or without finite losses
- Dealing with multi-scale geometries

Advantages Some of the notable features of ν FDTD are:

- Unlike the conventional FDTD, the mesh size utilized by the ν FDTD is not dictated by the finest feature of the geometry, and this size is usually maintained at the conventional $\lambda/20$ level. This helps to reduce the computational burden by a large factor.
- The ν FDTD algorithm incorporates a novel post-processing technique which requires relatively few time steps, in comparison to the number of steps required by the conventional FDTD to reach numerical convergence.

3. LOW-FREQUENCY RESPONSE

Despite many advances in Finite methods, such as the FEM and the FDTD, as well as in integral-equation-based techniques such as the MoM, accurately calculating the low frequency response for radiation and scattering problems continue to pose a challenge. The frequency domain techniques, such as the FEM and MoM, both experience difficulties at low frequencies, because they have to deal with ill-conditioned matrices at these frequencies. On the other hand, while the time-domain-based techniques, such as the FDTD, can accurately generate results at high frequencies, usually above 1 GHz, the same cannot be said about their performance at low frequencies. This is not only because the FDTD results are often corrupted by the presence of non-physical artifacts at low frequencies, but also because the FDTD requires exorbitantly large number of time steps for accurate calculation of the response. The required number of time steps can exceed a few million in some cases before convergence is achieved.

As an example, let us consider a 32-port connector circuit example shown in Fig. 1. This connector geometry has been analyzed by using a commercial FDTD solver and the variation of the transmission co-efficient S_{21} is plotted in Fig. 2 as a function of the frequency, and we observe that the results shows ripples that are numerical artifacts. Table 1 compares the number of time steps required for the solution to converge at different frequencies for the connector geometry. It can be inferred from this Table that the number of time steps required for the convergence increases as we go down in frequency, and eventually it becomes totally impractical to solve the problem at very low frequencies. Accurate calculation of the low-frequency response becomes especially critical in the area of RF and digital circuits, since inaccurate results can affect the causality behavior of the overall system. The ν FDTD utilizes a new technique, which is based on analytic continuation of the results derived at higher frequencies, and which is implemented by using the DM Approach and related techniques. This new technique is universal in nature, and it covers the entire range of frequencies, including the limiting case of $f \rightarrow 0$. Also, the ν FDTD can not only handle both the RF/Digital circuit problems, but also the radiation/scattering type problems with equal ease, by employing unique methodologies tailored for each of these categories. We present these methodologies in detail in the sections that follow.

Table 1. Comparison of time steps required for convergence for the circuit shown in Fig. 1.

Frequency	10 MHz	1 MHz	1 Hz
Time Steps in Millions	0.7	7	70

3.1. RF and Digital Circuits

Consider the variation of the isolation co-efficient S_{31} shown in Fig. 3 for the connector geometry (Fig. 1). This plot is divided into three regions, namely:

- Region-1: Low-frequency regime

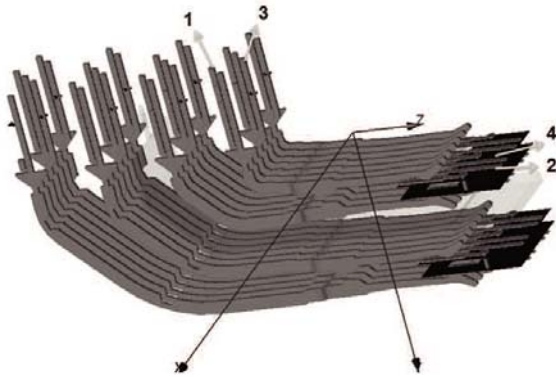


Figure 1. A 32-port connector with a overall dimension of $5.6 \times 11.88 \times 27.35$ mm (Housing not shown here).

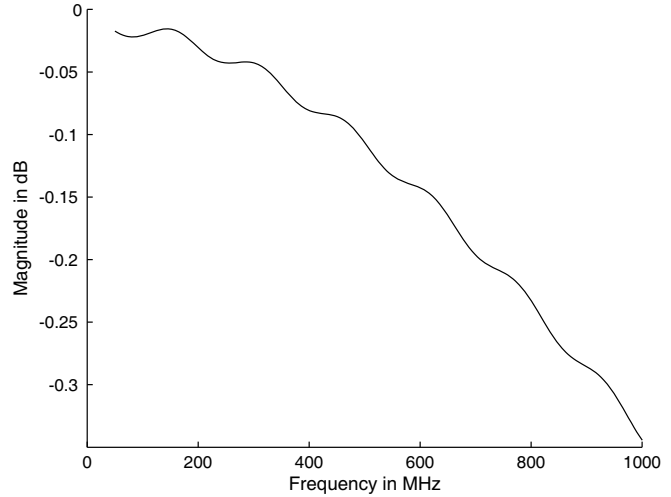


Figure 2. Variation of the transmission co-efficient S_{21} for the 32-port connector shown in Fig. 1.

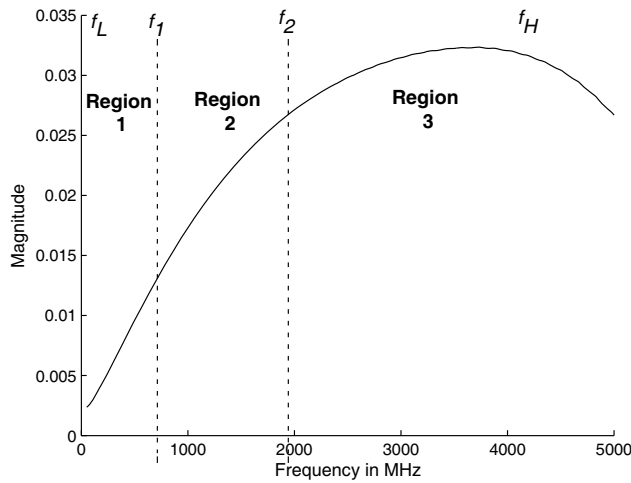


Figure 3. Variation of the isolation co-efficient S_{31} for the 32-port connector shown in Fig. 1.

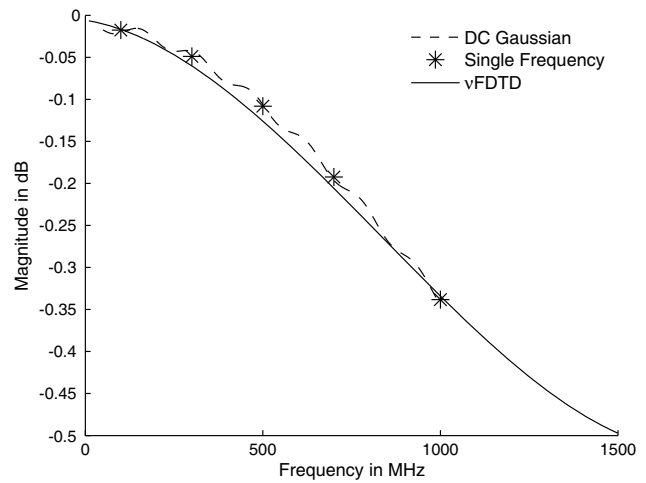


Figure 4. Variation of the transmission co-efficient S_{21} for the 32-port connector shown in Fig. 1 calculated using ν FDTD.

- Region-2: Validation region
- Region-3: High-frequency regime

There are four frequency values which delimit the above three regions. The frequency f_L describes the lowest frequency of interest defined by the user. The frequency f_1 , which divides the regions 1 and 2, is typically chosen to be between 500 MHz to 1000 MHz, while the frequency f_2 dividing the regions 2 and 3 is chosen to be on the order of $2f_1$ or $3f_1$. The frequency f_H is the user input indicating the highest frequency of interest. In each of these three regions the results are calculated by using a different method. The results in the high-frequency regime are generated by using the conventional FDTD, using a DC Gaussian pulse as the excitation source, whose 3 dB cut-off frequency is set to be f_H . In the low-frequency regime, the results are generated by using the proposed new technique, which involves the following steps:

- (i) Smooth the “DC Gaussian” Results.

- (ii) Fit the curve from f_L to f_1 with the DC values using a quadratic, for instance. The choice of f_1 can be fine-tuned based on the quality of the resulting fit.
- (iii) Validate the smoothed “DC Gaussian” results in region-2 by comparing them with those generated by “single frequency” simulations at a few points (typically 2 or 3).

We have recalculated the results for the 32-port connector geometry, shown in Fig. 1, by using the above method. The new results for the variation of the transmission co-efficient S_{21} and the isolation co-efficient S_{31} are shown in Figs. 4 and 5. From these figures we can clearly see that the conventional FDTD simulation utilizing the DC Gaussian pulse does not generate an accurate low-frequency response and has numerical artifacts, while the ν FDTD does not suffer from the same. These artifacts often introduce instabilities in the time domain when using SPICE-type simulation for instance.

For the next example, we consider an 8-port connector as shown in Fig. 6, which operates in the frequency range 50–800 MHz. Fig. 7 compares the variation of S_{31} calculated by using the ν FDTD with those obtained by using the DC Gaussian in the conventional FDTD algorithm. Again we find that the

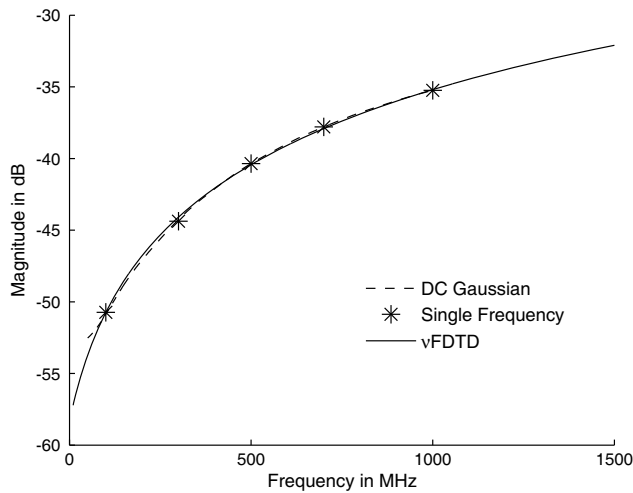


Figure 5. Variation of the isolation co-efficient S_{31} for the 32-port connector shown in Fig. 1 calculated using ν FDTD.

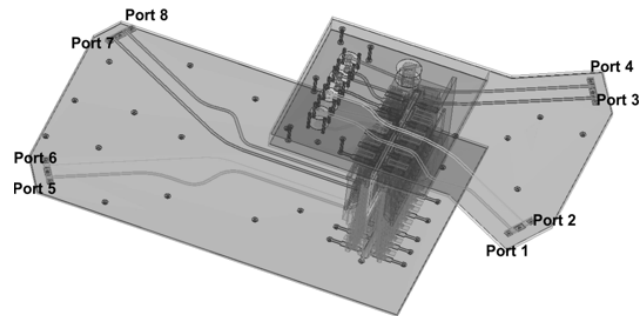


Figure 6. A 8-port connector (Housing not shown here).

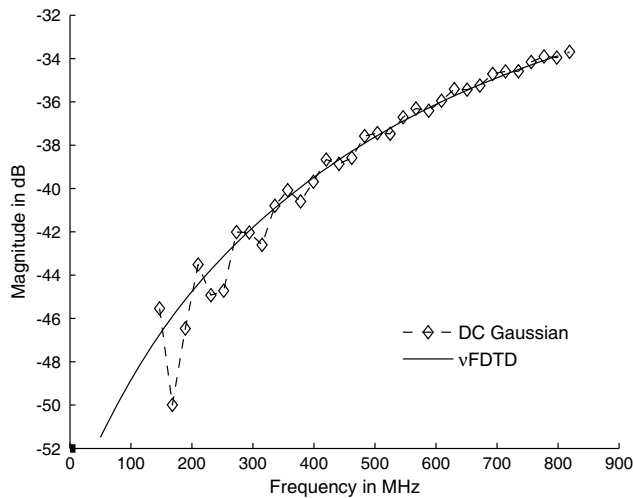


Figure 7. Variation of the S_{31} for the 8-port connector shown in Fig. 6.

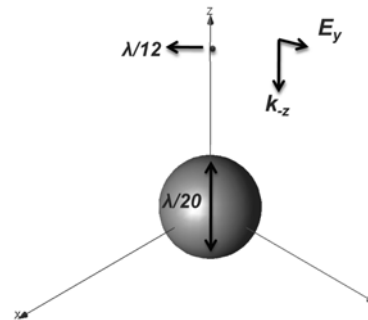


Figure 8. A PEC sphere of diameter $\frac{\lambda}{20}$ at 10 GHz.

DC Gaussian results show spurious spikes, while the ν FDTD is able to calculate it accurately.

3.2. Scattering Problems

In this section we turn to the solution of scattering problems by using the ν FDTD. The methodology for handling the radiation and scattering problems is different from that used for RF/Digital circuits, as we will explain below. For the high-frequency regime, we use the conventional FDTD and employ a Gaussian excitation source to generate the results. However, we utilize a different procedure, in the low-frequency regime, as outlined below:

- (i) Run a “Single Frequency” simulation at a frequency f_1 , where the largest dimension of the geometry is $\lambda/100$, to calculate the fields at a point located $\lambda/20$ from the surface of the object.
- (ii) Extract the dipole moment from the field values calculated above by using the analytical expressions for the fields radiated by an infinitesimal dipole [4].
- (iii) Use the extracted dipole moment to calculate the results from f_L to f_2 , where f_L is the lowest frequency of interest, and f_2 is typically chosen to be $2f_1$ or $3f_1$. It has been found that the results generated by using this dipole moment is not only valid for frequencies, even as low as 0, but also up to frequencies where the largest dimension of the geometry becomes $\lambda/10$; hence it enables us to seamlessly dovetail the low-frequency results with the lower end of the high frequency response.
- (iv) Validate the “DC Gaussian” results in the range between f_1 and f_2 by comparing them with those calculated by using the analytical expression at a few points (typically 2 or 3).

In order to extract the dipole moment from a single-frequency simulation, one can either use the method proposed by Furse [5], or use the DFT to process the time signature. In the Furse method, we choose two samples of the time signature and we fit the time signature to a sinusoidal curve using those two samples. Even though this method appears to be computationally inexpensive when compared to the DFT approach, the choice of the two samples determines the accuracy of the method, and these samples should not lie within the transient region; hence we always use the DFT to extract the DM because of its robustness.

As an example application of the procedure just outlined, we consider a sphere with a diameter of $\lambda/20$, with λ defined at 10 GHz. The sphere is illuminated by a plane wave traveling in the negative- z direction, with its E -field polarized along y . Fig. 9 compares the fields calculated by the proposed technique, in the frequency range of 1 Hz to 30 GHz, with those derived analytically. We find that the fields calculated by using the proposed technique based on DM extraction exhibits good agreement

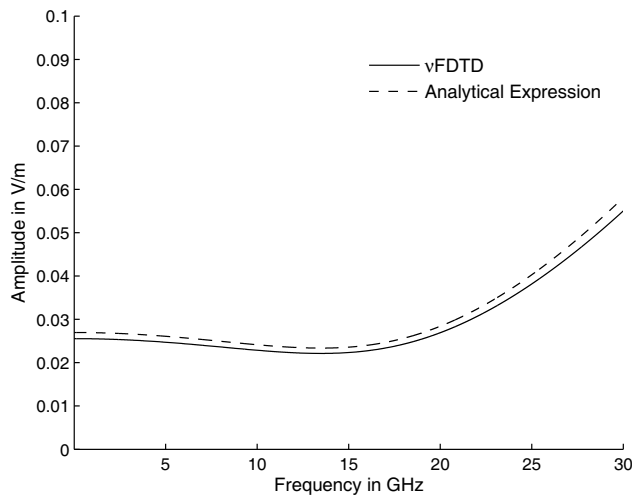


Figure 9. Amplitude variation of the scattered E_y at a point $z = 0.25$ cm with frequencies from 1 Hz to 30 GHz.

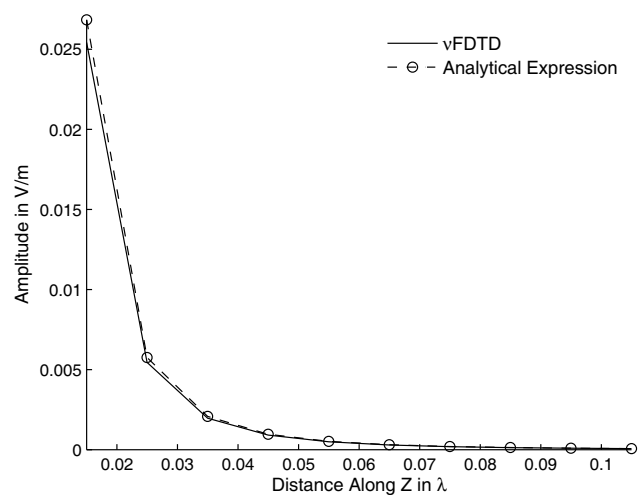


Figure 10. Amplitude variation of the scattered E_y with distance along z from $\frac{\lambda}{67}$ to $\frac{\lambda}{10}$, at 1.8 GHz.

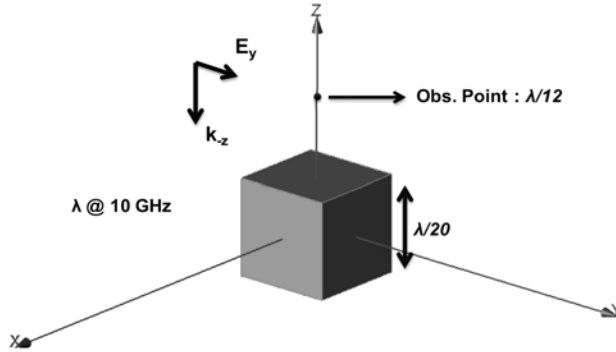


Figure 11. A PEC cube of side length $\frac{\lambda}{20}$ at 10 GHz.

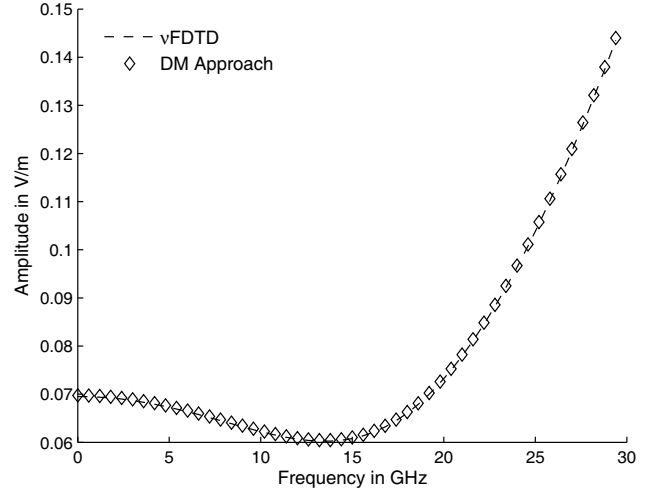


Figure 12. Amplitude variation of the scattered E_y at a point with frequencies from 1 Hz to 30 GHz.

with those calculated by using analytical expressions. The small deviation between the two curves is attributable to the staircase modeling of the sphere in the conventional FDTD, and it can be corrected by using an effective radius in the analytical expression. It is important to recognize the fact that we have used the same technique to calculate the response over the entire frequency range, including frequencies as low as 1 Hz, without using either the quasi-static approximation or other special treatments that are employed in the conventional computational electromagnetic (CEM) techniques. Even after the use of these special treatments in the existing techniques, such as the FEM and MoM, the accuracy of the low-frequency solution is often questionable because of the large condition numbers of the associated matrix. Thus, despite all the special treatments implemented in these methods to address the low-frequency breakdown problem, it is totally impractical to go down to frequencies on the order of 1 Hz in the existing techniques.

The amplitude variation of the scattered field with the distance along z , calculated by using the proposed technique, is shown in Fig. 10 for a frequency of 1.8 GHz. This plot also compares the results with those calculated by using analytical expressions. Again we find good agreement between the ν FDTD results and those generated from the analytical expression for a $\lambda/67$ sphere, for the chosen frequency of 1.8 GHz. The field variation derived by using the ν FDTD matches well with that generated from the analytical expression, both in the near and far field regions.

For the next example we consider the problem of scattering by a PEC cube of side length $\lambda/20$, as shown in Fig. 11; at a frequency of 10 GHz. Fig. 12 plots the scattered E_y -field as a function of frequency, calculated at $z = 2.5$ mm ($\lambda/12$ at 10 GHz) by using the ν FDTD, and compares it with the result obtained by using the DM approach. The comparison is seen to be good even at a frequency as low as 1 Hz.

Based on the illustrative examples presented above, we list below some of the advantages of the proposed method:

- RF and Digital Circuit Problems:
Efficient for constructing low-frequency solutions, compared to the long runs in FDTD.
- Scattering Problems:
 - (a) Can be used for *an arbitrary geometry*.
 - (b) Can be used to efficiently calculate not only the frequency response, but the *near and far fields* as well.

4. NON-CARTESIAN GEOMETRIES

The conventional FDTD uses a staircase approximation to model non-Cartesian geometries, as shown in Fig. 13, and requires the use of a very fine mesh to mitigate the effects of this staircase approximation when dealing with curved objects. This, in turn, makes the simulation computationally expensive, both in terms of memory and CPU time. Even though methods such as FEM and MoM can handle curved geometries with much ease because they do not restrict themselves to a Cartesian type of meshing, often they are not necessarily computationally efficient when dealing with inhomogeneous media. Hence, it would be advantageous to modify the existing FDTD algorithm so that it can handle curved geometries, enabling us to conveniently model arbitrary objects, regardless of their material parameters. In the past, a generalization of the conventional FDTD, namely the CFDTD algorithm [2], has been developed for this purpose. In CFDTD, the magnetic field update equations are modified by using the areas of the partially-filled cells, as opposed to those of the entire cells.

To explain the concept, we consider a partially-filled cell, shown in Fig. 14. The equation for this partially-filled cell is derived by using Farady’s law, to get:

$$\oint_{C_1} \vec{E} \cdot d\vec{l} = -\mu \frac{\partial}{\partial t} \int_{S_1} \vec{H} \cdot d\vec{s} \tag{1}$$

where C_1 is the loop ABCDA and S_1 is the area enclosed by loop C_1 . Upon discretizing this equation, we obtain:

$$H_z^{n+\frac{1}{2}}(i, j, k) = H_z^{n-\frac{1}{2}}(i, j, k) - \frac{dt}{\mu S_1} [-E_y^n(i, j, k) \cdot l_{AB} + E_x^n(i, j, k) \cdot dh + E_y^n(i + 1, j, k) \cdot l_{CD}] \tag{2}$$

The update magnetic equation for the partially-filled cell is shown above in (2). But, as $S_1 \rightarrow 0$, this modified update equation becomes unstable because, as we see from (2), the expression for the updated H contains S_1 in the denominator. The update equation can be modified to circumvent this instability problem that arises when the partial area is small, albeit at the cost of compromising the accuracy. Hence, in order to improve the accuracy, we propose two new approaches for handling non-Cartesian geometries, as explained below.

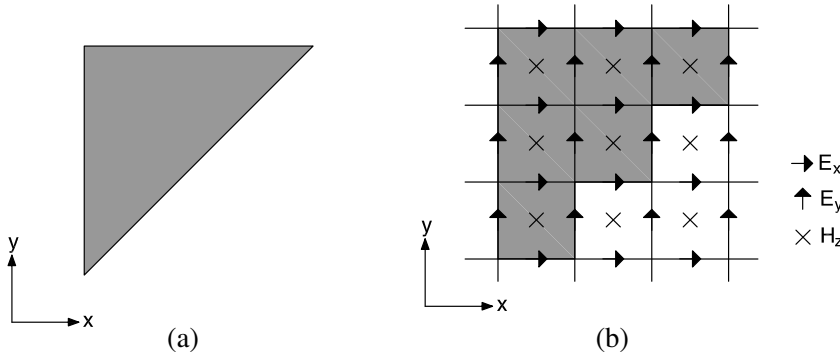


Figure 13. Meshing of a non-Cartesian geometry by the conventional FDTD. (a) A PEC wedge geometry. (b) A PEC wedge with staircase approximation.

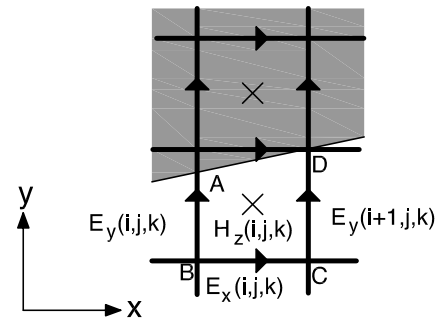


Figure 14. A partially-filled cell.

4.1. Asymptotic Method

In this asymptotic type of implementation, the field values as opposed to the update equations, are modified by using the local field solution. The proposed new technique is described below:

- For the partially-filled cells with a fill factor $\leq 50\%$, the E -fields are updated by using the H -fields derived from the modified CFDTD equation given in (2).

- For the partially-filled cells with a fill factor $> 50\%$, the E -fields are updated by using local solutions, generated on the basis of concepts of reflection or diffraction, rather than the use of the H -fields employed in the CFDTD approach.

Because we use the asymptotic method to compute the reflection or diffraction coefficients, the proposed technique requires a “single-frequency” simulation. However, this technique can be extended to “DC Gaussian” simulations with a slight modification as described next in the Section 4.2. Also, the proposed technique can be extended to dielectrics and inhomogeneous geometries without any modification, while the CFDTD cannot handle either of them without compromising the accuracy.

Let us consider the case of a square PEC sheet whose sides are approximately 4λ (λ referenced at 10 GHz) that are inclined at an angle of 0.72° with respect to the x -axis, as shown in Fig. 15. The tilt angle has been chosen to be 0.72° so that the edges of the sheet are offset only by $\pm\lambda/40$ above or below the x -axis, i.e., half the FDTD cell size of $\lambda/20$. We calculate the amplitude variation of the scattered E_x field at a frequency of 10 GHz, when the plate is illuminated by a plane wave, which travels along the negative- y direction and is polarized along x . Fig. 16 compares the results obtained by using the proposed technique, with those returned by the CFDTD, and by a commercial MoM code, for the same problem. The results generated by using the proposed technique show good agreement with the results from the commercial MoM code, while the CFDTD results exhibits spurious ripples in the lit region because of the instability problem it encounters when the area $S_1 \rightarrow 0$. Moreover, this is true even when a fine mesh size of $\frac{\lambda}{160}$ is used in the CFDTD, in contrast to the $\frac{\lambda}{20}$ mesh size used in ν FDTD. Table 2 presents a comparison of the mesh size and the memory requirements, and shows that the proposed technique easily out-performs the CFDTD, which still suffers from inaccuracies, even when a very fine mesh is used.

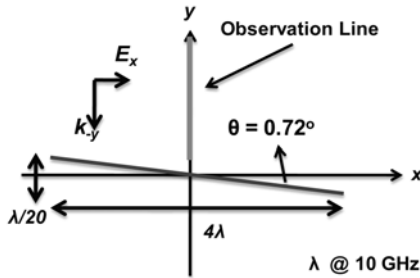


Figure 15. A inclined PEC sheet (not to scale).

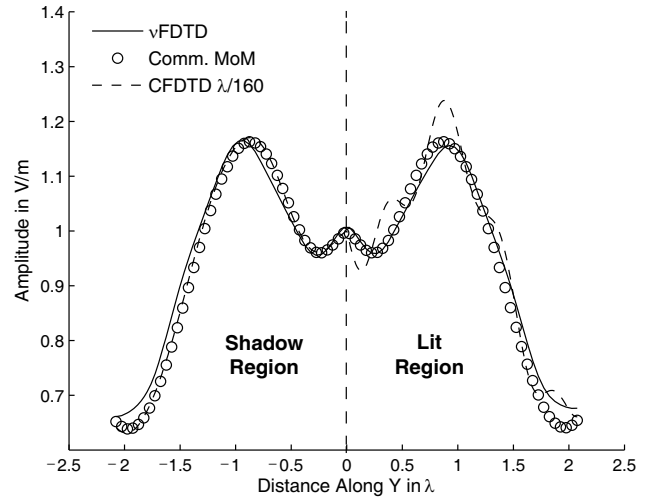


Figure 16. Amplitude variation of the scattered E_x with distance along y at 10 GHz.

Table 2. Comparison of mesh size and memory required for convergence for PEC geometry shown in Fig. 15.

Parameter	ν FDTD	CFDTD ^a
Mesh Size Used	$\frac{\lambda}{20}$	$\frac{\lambda}{160}$
Memory Required	413 MB	31 GB

^a Results still have numerical artifacts

For the next example, let us change the inclination of the PEC plate in the previous problem from 0.72° to 1.43° . Fig. 17 compares the scattered E_x -field calculated by using the ν FDTD/Asymptotic method, with those obtained by using the CFDTD algorithm with a mesh size of $\lambda/160$, and with the

commercial MoM code results. We again find that the results from the ν FDTD match well with those obtained by using the commercial MoM code, while the results from the CFDTD show spurious ripples due to the instability problem alluded to above.

For the next example, we consider a faceted PEC surface (see Fig. 18) whose projected length is λ at a frequency of 10 GHz. Fig. 19 compares the backscattered E_z -field calculated by using the ν FDTD with those obtained from: (i) the CFDTD with a mesh size of $\lambda/20$; (ii) a commercial MoM code; and (iii) a commercial FEM. Again we find that the results calculated by using the ν FDTD compares well with those obtained from the commercial MoM code, while the results from the commercial FEM code shows numerical artifacts.

For the next example, let us consider a PEC wedge of side length 4λ , as shown in Fig. 20. Fig. 21 plots the scattered field at a frequency of 10 GHz along the specular direction, obtained by using the ν FDTD, and compares it with those obtained by using the CFDTD with a mesh size of $\lambda/50$; with a commercial MoM code; and, with a commercial FEM code. We find a good comparison between the scattered field calculated by using the ν FDTD with that obtained from the commercial MoM code,

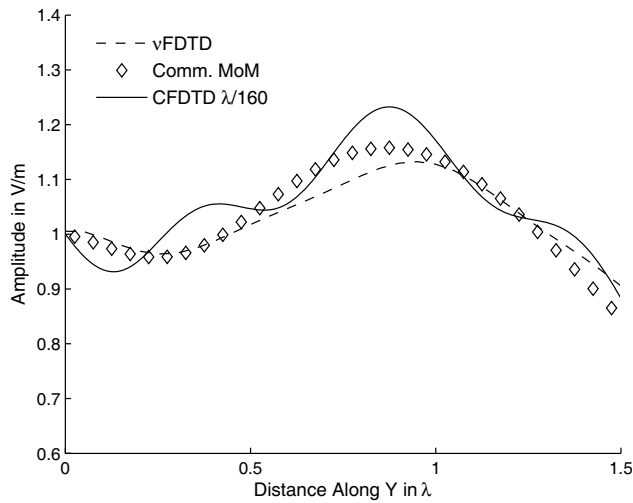


Figure 17. Amplitude variation of the scattered E_x with distance along y at 10 GHz.

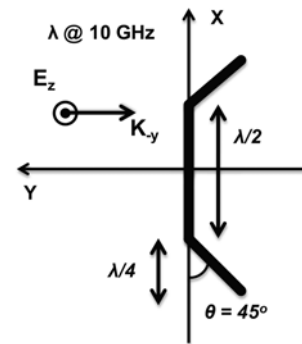


Figure 18. A faceted PEC surface (not to scale).

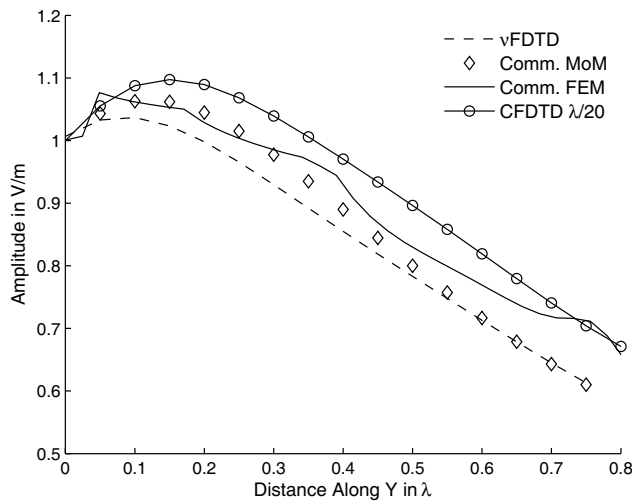


Figure 19. Amplitude variation of the backscattered E_z with distance along y at 10 GHz.

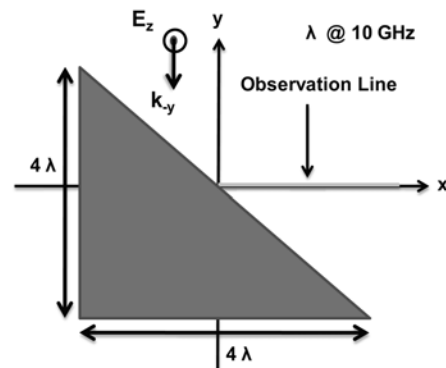


Figure 20. A PEC wedge.

while the results from the CFDTD and the commercial FEM codes show spurious ripples.

For our next example, we consider a finite PEC cylinder, as shown in Fig. 22, which has a height of $21\lambda/20$ at a frequency of 10 GHz, for the next example. In order to calculate the field in the asymptotic limit in the ν FDTD method, we use the fields scattered by an infinite PEC sheet multiplied by the factor f , defined in (3)

$$f = \sqrt{\frac{a'}{r}} \tag{3}$$

where a' is the effective phase center and r the distance of the observation point from the effective phase center. A wide range of numerical experiments has shown that this effective phase center for a PEC cylinder is always $0.5a$, where a is the radius of the cylinder.

Figure 23 compares the backscattered E_z -fields calculated by using the ν FDTD with those obtained from the CFDTD with a mesh size of $\lambda/20$; with a commercial MoM code; and, with a commercial FEM code. We find that the fields calculated by using the ν FDTD compare well with those obtained by using the commercial MoM solver. The results calculated using the commercial FEM shows numerical

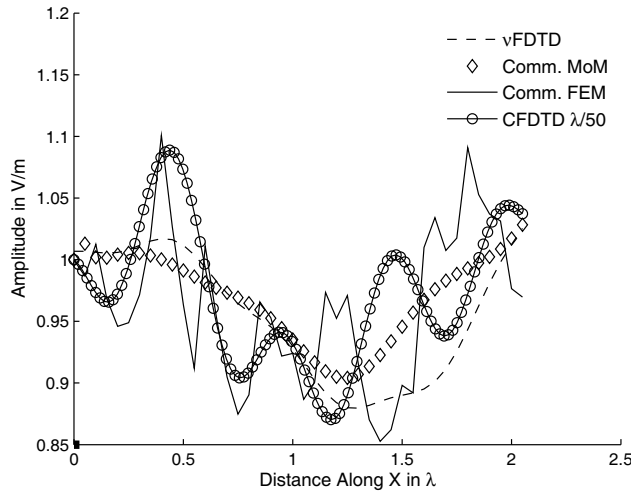


Figure 21. Amplitude variation of the scattered E_z with distance along x at 10 GHz.

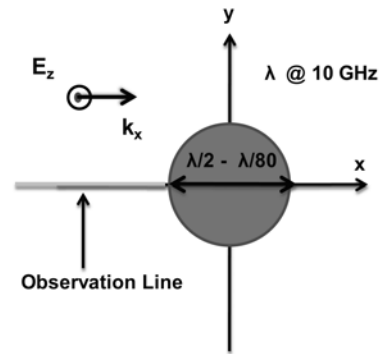


Figure 22. A PEC cylinder.

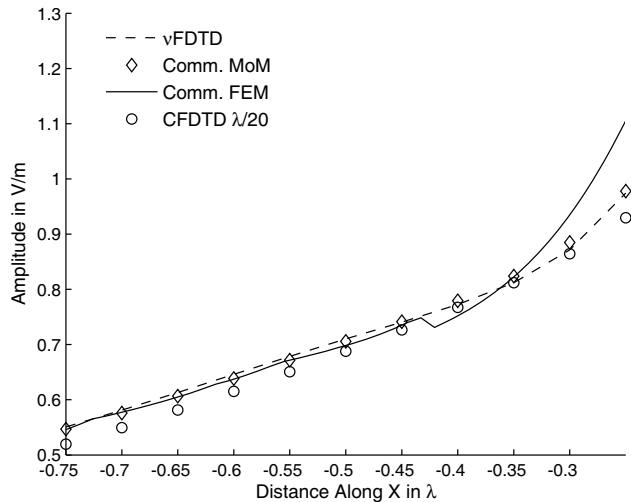


Figure 23. Amplitude variation of the backscattered E_z with distance along x at 10 GHz.

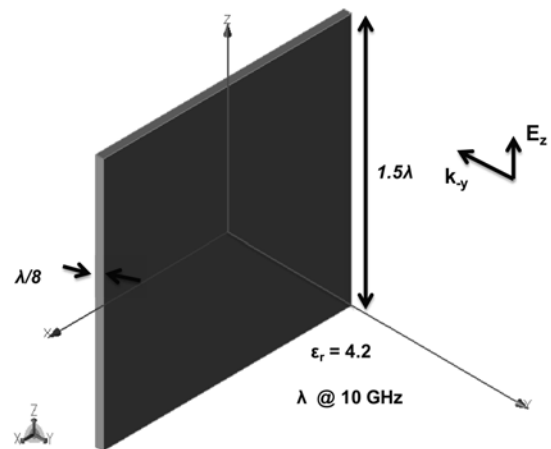


Figure 24. A thin dielectric slab (not to scale).

artifacts and the CFDTD does not generate the correct scattered field on the surface of the cylinder; however the ν FDTD is able to solve this problem with good accuracy.

While modeling dielectric objects using the CFDTD approach, the medium parameters in the partially-filled cells are replaced by an average dielectric constant over the entire volume of the cell. The asymptotic method proposed here in can be used as an alternative approach to model dielectric objects without any modifications, and with better accuracy than that of the CFDTD method. As an example, let us consider the dielectric slab of thickness $\lambda/8$ at a frequency of 10 GHz, with $\epsilon_r = 4.2$ as shown in Fig. 24. Fig. 25 compares the backscattered E_z -field calculated by using the ν FDTD with those generated by using the CFDTD, and with the commercial FEM code. We find that the results generated by using the commercial FEM and CFDTD codes exhibit spurious ripples, while those from the ν FDTD have a smooth behavior, which is realistic.

In order to demonstrate the efficacy of the ν FDTD method, we vary the thickness of the slab, and choose it to be $9\lambda/80$, $10\lambda/80$ and $11\lambda/80$ at a frequency of 10 GHz. We calculate the phase variation at $y = \lambda/40$ and plot it in Fig. 26, which shows the comparison of the phase variation against the thickness, generated by using the infinite slab analytical expression; the CFDTD; and a commercial FEM code. We find that the results calculated by using the ν FDTD compares well with those derived from the analytical expressions for the infinite slab, while the results generated by using the other methods deviate from the analytical results.

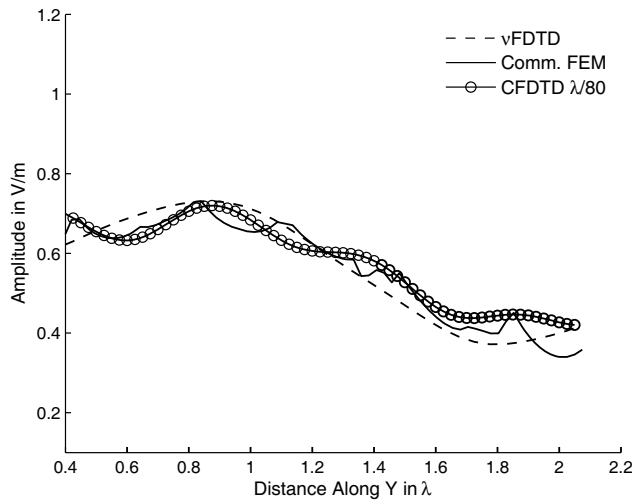


Figure 25. Amplitude variation of the backscattered E_z with distance along y at 10 GHz.

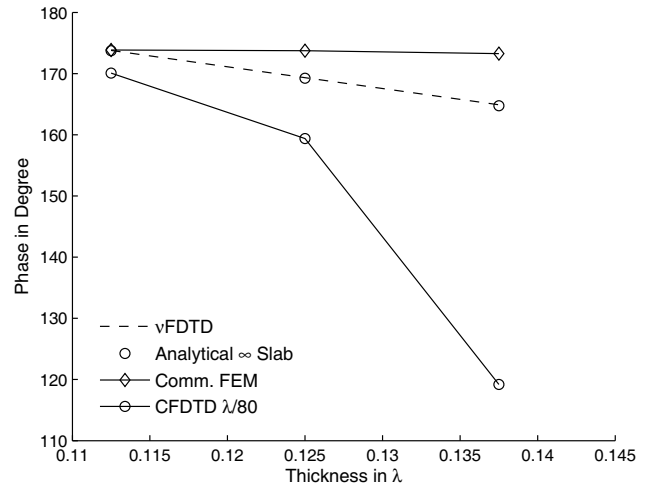


Figure 26. Phase variation of the backscattered E_z at $y = \lambda/40$.

4.2. Averaging Technique

As mentioned in Section 4.1, the proposed ν FDTD technique requires a “single frequency” simulation because we use the asymptotic limit to compute the reflection or diffraction coefficients. In this section, we describe a modified approach in which we use the “DC Gaussian” simulation that enables us to generate results for a wide range of frequencies. In order to demonstrate the usefulness of this approach, we consider the example of a rectangular cylinder of height 4λ at a frequency of 10 GHz, which has mitred corners as shown in Fig. 27. The problem is handled in three steps as shown in Fig. 28 and we use scattered-field type of formulation in all of these steps. Even though it shows three steps, it is important to note the fact that we need only two simulations, since the calculation of the scattered field in step-2 is trivial when the boundary condition on the PEC is used. The simulation for the first step does not call for any modifications to the FDTD algorithm. However, for the third step we need to modify the field value at the nodes of the partially filled cells by using the weighted average of the fields at these nodes, obtained from steps 1 and 2, based on the partially filled space in the actual geometry.

Figure 29 compares the backscattered E_y -field calculated by using the ν FDTD with that generated

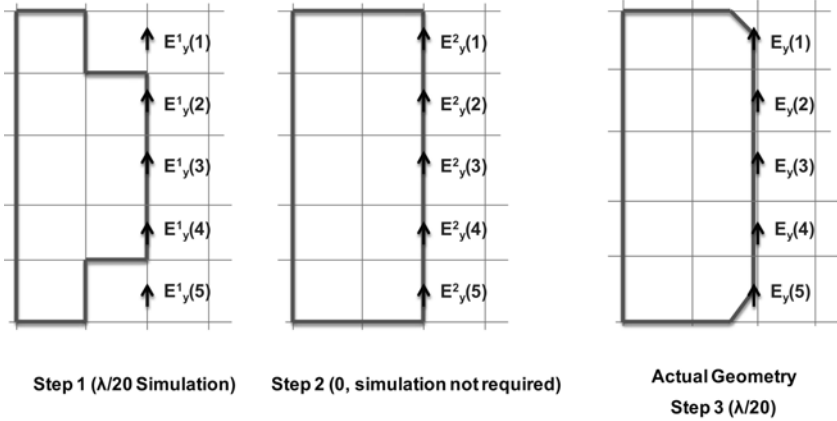
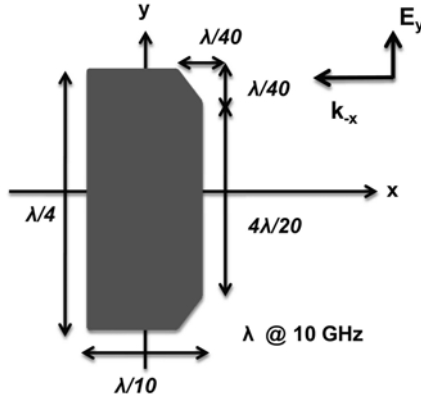


Figure 27. A PEC rectangular cylinder with mitered corner.

Figure 28. Principle behind the averaging technique.

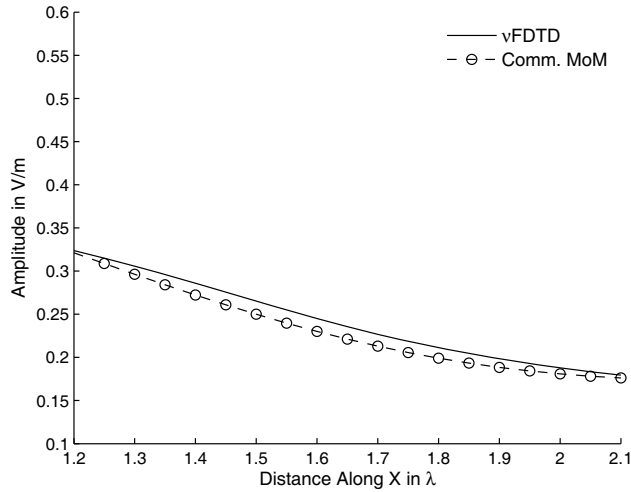


Figure 29. Amplitude variation of the backscattered E_y with distance along x at 10 GHz.

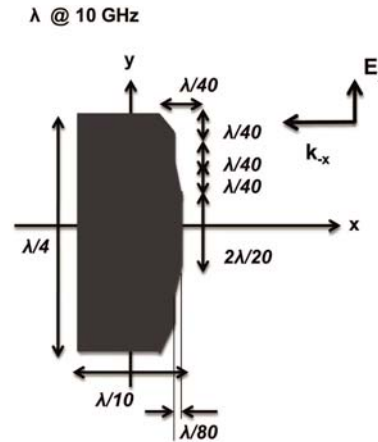


Figure 30. A faceted PEC geometry (not to scale).

by using the commercial MoM code, and the comparison is seen to be good. For the next example, we consider the faceted PEC geometry shown in Fig. 30, whose projected footprint is 4λ at a frequency of 10 GHz. Fig. 31 compares the backscattered E_y -field, calculated by using the ν FDTD/Averaging technique, and with that obtained from a commercial MoM solver. From Fig. 31, we find that the solution generated by using the commercial MoM code shows a spurious spike near the surface of the geometry, while the ν FDTD results are smooth.

For the last example, we consider a curved PEC surface of height 4λ at a frequency of 10 GHz, as shown in Fig. 32. Fig. 33 compares the scattered E_y -field calculated by using the ν FDTD method, and with that from a commercial MoM code, and once again we find that the comparison is good.

4.3. Advantages

Below, we summarize some of the advantages of the proposed method:

- (a) Usable for *arbitrary geometries*, even if the surfaces do not coincide with the Cartesian mesh, e.g., thin sheets, with or without a slant.
- (b) More accurate than the conventional Conformal FDTD.
- (c) Retains $\lambda/20$ cell size even for thin, slanted and curved bodies, offering memory advantage and computational efficiency over conventional conformal FDTD.

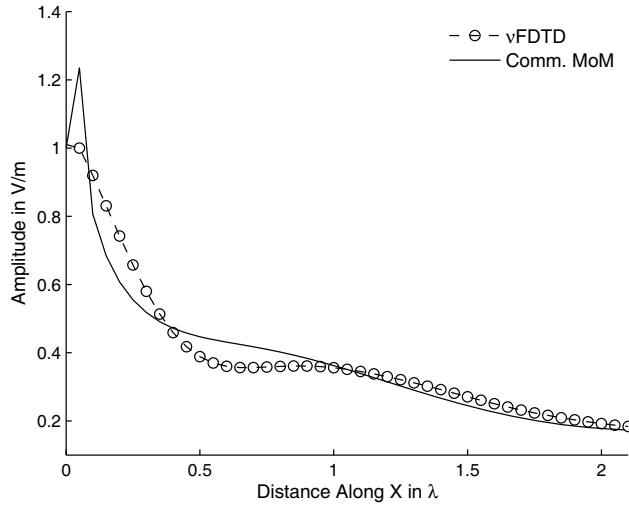


Figure 31. Amplitude variation of the backscattered E_y with distance along x at 10 GHz.

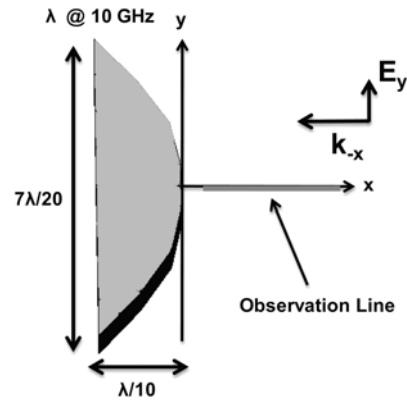


Figure 32. A curved PEC surface (with a height of 4λ).

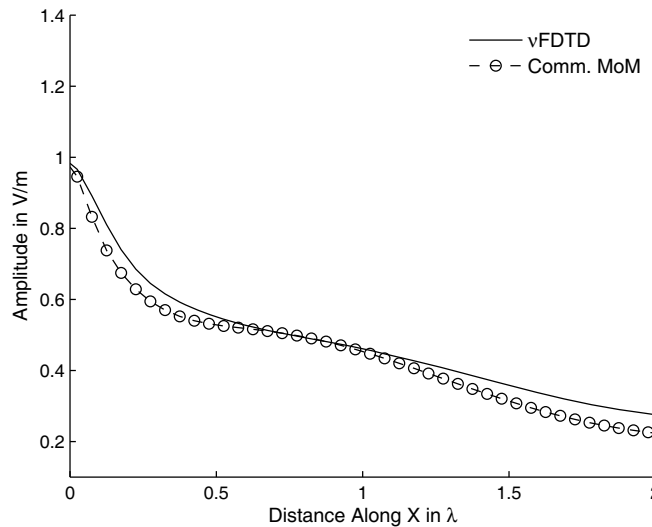


Figure 33. Amplitude variation of the scattered E_y at 10 GHz.

- (d) Free of instability problems even when the fractional area of the partially filled cell is very small, even when it tends to zero.
- (e) Can be extended to dielectric objects, with just a few modifications.

5. OBSERVATIONS AND CONCLUSIONS

In this article, we have introduced the ν FDTD solver, which is a blend of time and frequency domain techniques designed to generate accurate electromagnetic responses at low frequencies; deal with non-Cartesian geometries accurately without any instability issues that are often encountered in the conventional CFDTD; and, handle lossy/lossless thin structures with ease. In all of the cases for which we have carried out comparison studies with the existing algorithms and commercial codes, the ν FDTD was not only accurate but also computationally the most efficient. Finally, since ν FDTD builds on the conventional FDTD to solve different types of problems, its performance can be further enhanced by

parallelizing the algorithm [6], which can be carried out as easily as in the case of the conventional FDTD.

REFERENCES

1. Mitra, R., *Computational Electromagnetics: Recent Advances and Engineering Applications*, Springer-Verlag, New York, USA, 2013.
2. Yu, W. and R. Mitra, "A conformal FDTD software package modeling antennas and microstrip circuit components," *IEEE Trans. Antennas and Propagation*, 28–39, 2000.
3. Panayappan, K., "Novel frequency domain techniques and advances in finite difference time domain (FDTD) method for efficient solution of multiscale electromagnetic problems," Ph.D. dissertation, The Pennsylvania State University, University Park, May 2013.
4. Balanis, C. A., *Antenna Theory: Analysis and Design*, John Wiley & Sons, New Jersey, 2005.
5. Furse, C. M., "Application of the finite difference time domain method to bioelectromagnetic simulations," *Applied Computational Electromagnetics Society Newsletter*, 1997.
6. Yu, W., R. Mitra, T. Su, Y. Liu, and X. Yang, *Parallel Finite-Difference Time-Domain Method*, Artech House, London, 2006.